



**HAL**  
open science

## Dynamical buckling of a table-tennis ball impinging normally on a rigid target: experimental and numerical studies

Théophile Rémond, Vincent Dolique, Franck Vittoz, Sheedev Antony, Renaud G Rinaldi, Lionel Manin, Jean-Christophe Géminard

### ► To cite this version:

Théophile Rémond, Vincent Dolique, Franck Vittoz, Sheedev Antony, Renaud G Rinaldi, et al.. Dynamical buckling of a table-tennis ball impinging normally on a rigid target: experimental and numerical studies. *Physical Review E* , 2022, 106 (1), pp.014207. 10.1103/PhysRevE.106.014207 . hal-03718994

**HAL Id: hal-03718994**

**<https://hal.science/hal-03718994>**

Submitted on 10 Jul 2022

**HAL** is a multi-disciplinary open access archive for the deposit and dissemination of scientific research documents, whether they are published or not. The documents may come from teaching and research institutions in France or abroad, or from public or private research centers.

L'archive ouverte pluridisciplinaire **HAL**, est destinée au dépôt et à la diffusion de documents scientifiques de niveau recherche, publiés ou non, émanant des établissements d'enseignement et de recherche français ou étrangers, des laboratoires publics ou privés.

# Dynamical buckling of a table-tennis ball impinging normally on a rigid target: experimental and numerical studies

Théophile Rémond<sup>1</sup>, Vincent Dolique<sup>1</sup>, Franck Vittoz<sup>1</sup>, Sheedev Antony<sup>2</sup>,

Renaud G. Rinaldi<sup>3</sup>, Lionel Manin<sup>2,†</sup>, and Jean-Christophe Géminard<sup>1</sup>

<sup>1</sup> LPENSL, CNRS UMR5672, ENS de Lyon, F-69342 Lyon, France

<sup>2</sup> LaMCoS, CNRS UMR 5529, INSA-Lyon, Univ Lyon, F-69621 Villeurbanne, France

<sup>3</sup> MATEIS, CNRS UMR 5521, INSA-Lyon, Univ Lyon, F-69621 Villeurbanne, France

(Dated: June 19, 2022)

We report on the dynamical buckling of a spherical shell (a table-tennis ball) impinging in normal incidence on a rigid surface (a glass plate). Experimentally, we observe and decipher the geometrical characteristics of the shell profile in the contact region along with global metrics such as the contact duration and the coefficient of restitution of the linear velocity. We determine, in particular, the onset of the ball buckling instability. We find that, just like in quasi-statics, the shell buckles when the crushing exceeds about twice the thickness of the shell. In addition, for launching conditions resulting in the ball elastic buckling, a drop of the restitution coefficient is observed. A companion numerical Finite Elements study is set to monitor the different sources of energy and reveals that the added energy loss is mainly due to the friction between the shell surface and the solid substrate.

## I. INTRODUCTION

The rebound of the table-tennis ball off the paddle is among the common examples of the impact of a thin-walled hollow sphere onto a solid body, more or less rigid. Such hollow structures are indeed interesting for many engineering applications. Very common examples are vessels, containers, submarines, aircraft, etc. These structures can sustain important loads in spite of their small mass. However, they can be subjected to dramatic instabilities such as buckling in response to external loading, which compromises the integrity of the structure [1].

It has long been known that, even at moderate incident velocity, the shell of the table-tennis ball buckles on impact with the paddle [2–4]. Thus the ability of the paddle to give or stop spin and/or linear velocity greatly depends on the mechanical properties of the ball shell as well [5]. The spherical shell is one of the simplest models to study the buckling instability of curved structures. The study of the buckling under a quasi-static load has been the subject of several numerical, theoretical [6–10], and experimental studies [10–13]. The main result is that the onset of the instability is reached when the displacement of the shell towards the surface is about twice the shell thickness, yet slightly dependent on the radius of the shell and on the Poisson ratio of the ball parent material [3]. Note that a precise determination of the onset can be used to assess the properties of the material of the shell [14]. At larger deformation, far above the onset, the contact region loses its initial axi-symmetry [8], but this regime is out of the scope of the present paper.

Here, we are interested in the dynamical counterpart of these studies. We mean here by dynamic regime, a regime where the viscous effects could play a role and/or the contact time comparable to the period of a vibration mode of the spherical shell. Many authors have focused on the dynamical crushing of spherical shells because of the particular interest these structures present for building energy dampers [15–18]. That phenomenon involves mainly the plasticity of the structure that is used to best dissipate the energy. We shall consider

the opposite limit in which the initial energy is almost entirely recovered after impact. More precisely, we will consider the impact, in normal incidence, of a table-tennis ball onto a rigid and flat surface, and focus on the restitution of the kinetic energy in relation with the buckling of the shell. Former studies reported that the buckling onset is reached even at moderate (between  $3.5 \text{ m.s}^{-1}$  and  $5 \text{ m.s}^{-1}$ ) impact velocity [2, 3, 19], but they did not provide a direct determination of the shell profile during the collision, which is the main contribution of the present work.

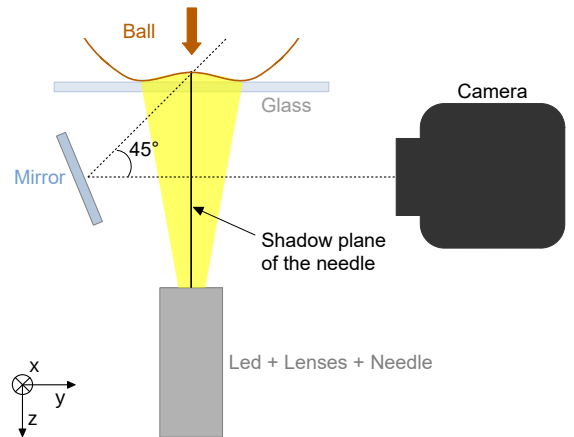


FIG. 1. Sketch of the observation technique – The ball is observed from below through the glass window and its profile in the contact region is assessed thanks to the use of the shadow of a needle cast onto the ball surface.

During the impact, the initial kinetic energy of the ball is mainly transferred into elastic energy associated to the shell deformation and converted back into kinetic energy as the ball bounces back from the surface, (almost) recovering its initial spherical shape [3]. However, there is always energy loss associated with the ball rebound, which leads to a reflected ve-

locity smaller than the incident velocity. There are several potential sources of energy loss. First, the shell might leave the surface without having entirely recovered its initial shape and take away a significant amount of energy loaded in its remaining elastic deformation. Second, due to the collision, the paddle and the substrate can vibrate and part of the initial energy can be mechanically radiated [20, 21]. There are at least two other potential sources of dissipation, related to the intrinsic dissipative nature of the system. On the one hand, the parent materials of the ball and of the paddle are visco-elastic and part of the energy might be transferred into heat. On the other hand, there might be a relative displacement of the shell and paddle surfaces that are at contact during the collision, and energy might be dissipated by friction [11, 22]. One can wonder how the buckling of the shell alters the respective contribution of these mechanisms in the decrease of the kinetic energy of the ball before and after collision.

## II. EXPERIMENTAL STUDY

### A. Experimental Principle and Setup

The experiment consists in observing the deformation of a table-tennis ball colliding in normal incidence with a rigid surface.

The homemade experimental setup makes it possible to launch the ball at a chosen velocity, without spin, along the vertical axis and then to observe the collision through the horizontal and transparent surface (a firmly held 2.8 mm-thick transparent glass window) it collides with (Fig. 1).

The ball (Cornilleau™, P-ball 3 stars, 4 cm-in-diameter, mass 2.7 g, ABS plastic, Table I) is launched downwards using a striker consisting of a metal rod driven by a spring. The system is initially armed by compressing the spring. The ball is then put into place in a holder underneath. The striker is subsequently released. The ball reaches the glass window with a vertical incident velocity,  $v_i$ , which typically ranges from  $1 \text{ m}\cdot\text{s}^{-1}$  to  $12 \text{ m}\cdot\text{s}^{-1}$  depending on the initial compression of the spring.

In order to assess the profile of the ball in the contact region, we used the light of a powerful LED (Luxeon Rebel ES, LXML-PWN2, 230 lm) and two optical lenses (Thorlabs, N-BK7 Bi-Convex Lenses, focal lengths 50 mm and 25.4 mm) to cast the shadow of a steel needle onto the ball surface, along the vertical axis (the needle is oriented along the  $x$ -axis). The ball surface, in the contact region, is observed at 45 deg with a fast camera (Kron Technologies, Chronos 2.1-HD, monochrome image sensor, 20,000 fps). For practical reasons, we use a mirror angled at 22.5 deg with respect to the vertical; the optical axis of the camera is horizontal. Images recorded at different times during the test are displayed in Fig. 2 and the shadow of the needle appears as a dark line on the bright surface of the ball. Due to the geometry of this experimental configuration, the profile of the ball surface is obtained by applying to the image a  $\sqrt{2}$  factor to the  $z$ -axis.

For each image, the profile of the shell is determined as follows (Fig. 3). The image is stretched by a factor  $\sqrt{2}$  in the  $z$

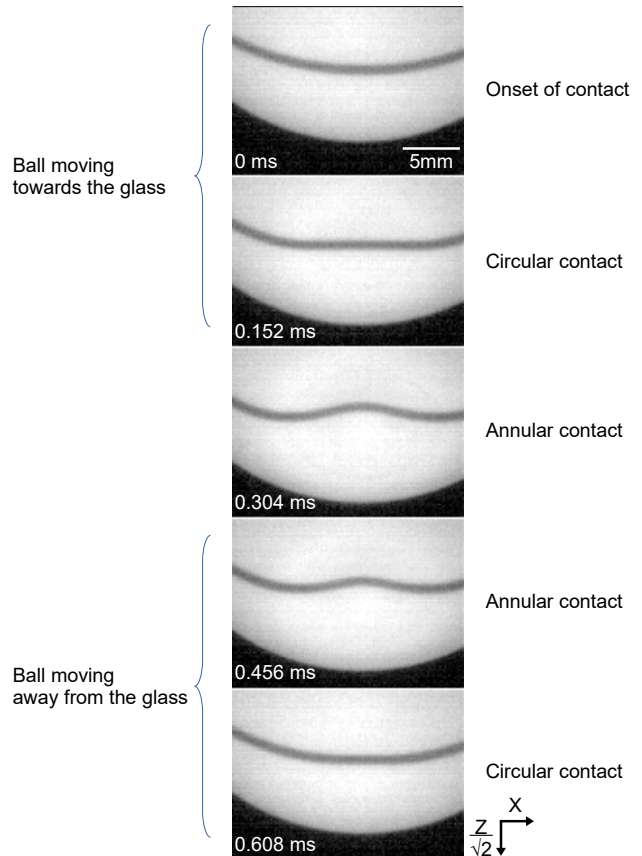


FIG. 2. Series of images of the ball surface during the collision with the glass window – The dark line, the shadow of a needle cast onto the ball surface, reveals the profile of the shell in the contact region [ $v_i = 9.7 \text{ m}\cdot\text{s}^{-1}$ ]. Time 0 ms coincides with the onset of contact.

direction (bicubic interpolation in ImageJ [23]). A Gaussian filter is applied in order to reduce the noise. Then, for each horizontal position  $x$ , the height of the shell above the substrate,  $z$ , corresponds to the darkest point encountered along the vertical axis. The resulting experimental profile  $z(x)$  is then interpolated to a polynomial of order 8 (dashed line in Fig. 3), symmetric with respect to point B (at center of the contact region, the position of the latter being a fitting parameter). The points A and C are defined as the limits of the contact region whose coordinates are then obtained analytically. We subsequently determine the relevant geometrical characteristics of the shell profile, in particular the diameter  $D$  of the contact region and the depth  $d$  of the buckled region (the height of point B above the glass window).

The velocity of the ball before,  $v_i$ , and after,  $v_r$ , it enters into contact with the surface are measured using the same image sequence (the same geometrical factor,  $\sqrt{2}$ , is applied). Both velocities are evaluated at contact since the acceleration due to gravity cannot be neglected. We characterize the energy loss by measuring the restitution coefficient of the normal velocity,

Geometrical properties			Material properties					
Diameter	Thickness	Mass	Density	Poisson ratio	Long-time modulus	Maxwell modulus	Relaxation time	Friction coefficient
$2R$	$h$	$m$	$\rho_b$	$\nu_b$	$E_\infty$	$E_1$	$\tau_1$	$\mu$
40 mm	0.5 mm	2.7 g	1070 kg.m <sup>-3</sup>	0.35	1.5 GPa	0.5 GPa	0.001 s	0.75

TABLE I. Ball properties: geometry and parent material.

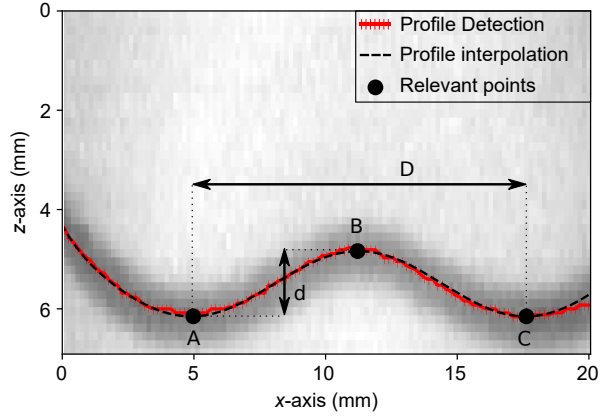


FIG. 3. Relevant characteristics of the shell profile – Once the profile of the shell is obtained (dashed line which interpolates the red line), we determine the position of points A and C that limit the contact region and the point B at center. Points A and C are used to assess the diameter  $D$  of the contact region, whereas the vertical distance between point B and line (AC) corresponds to the depth  $d$  of the buckled region [ $v_i = 9.7 \text{ m.s}^{-1}$ ,  $t = 0.355 \text{ ms}$  in Fig. 2].

$\varepsilon \equiv \frac{v_r}{v_i}$ . With account for the depicted experimental setup,  $\varepsilon$  is a unitless parameter with values ranging between 0 (the ball is stopped) and 1 (no energy loss).

## B. Experimental results

We use the experimental setup to study the dynamics of the ball collision over the whole range of the accessible velocities,  $v_i$ .

On the images (not shown here), one qualitatively observes that the contact region remains flat and circular only at small velocity  $v_i$ , typically less than 5 - 6  $\text{m.s}^{-1}$ . This is clearly observed in Fig. 4(a), in which the depth  $d$  is reported as a function of time  $t$  for different incident velocities  $v_i$  during the contact between the ball and the glass plate (contact duration of about 0.6 ms). Indeed, for  $v_i = 4.4 \text{ m.s}^{-1}$ ,  $d$  remains almost zero throughout the impact, whereas for  $v_i = 6.6 \text{ m.s}^{-1}$ ,  $d$  reaches a significant maximum of about half a millimeter.

We report in Fig. 4(b), the diameter  $D$  of the contact region as a function of time  $t$ . We can estimate from the diameter  $D$  of the contact region and from the ball radius  $R$ , the displacement of the ball towards the glass plate, or deflection  $\delta$ .

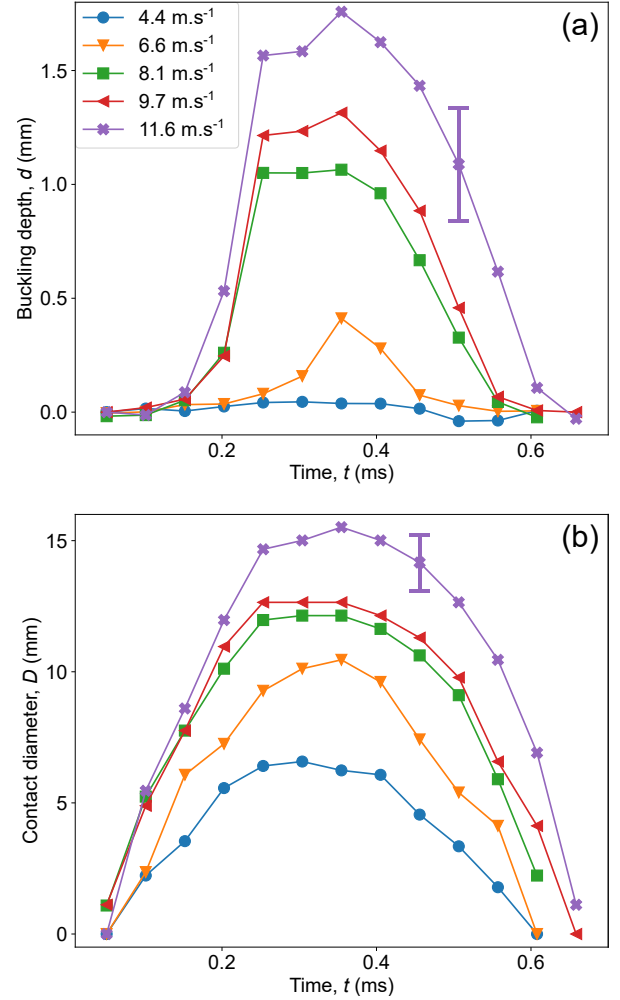


FIG. 4. Diameter  $D$  and depth  $d$  of the buckle vs time  $t$  – In (b), one observes that for velocities  $v_i$  above typically 5  $\text{m.s}^{-1}$ , the ball shell loses contact with the glass plate at center of the contact region. From the diameter  $D$  of the contact region, one can easily estimate that the contact time remains of the order of 0.6 ms.

Indeed, assuming a Hertz contact [24], we have:

$$\delta \simeq \frac{D^2}{4R}. \quad (1)$$

This relation is only valid when considering a Hertz contact, before the buckling instability occurs. We shall use the result to estimate the deflection  $\delta$  below the buckling onset and the buckling onset itself, which is correct. For the sake of sim-

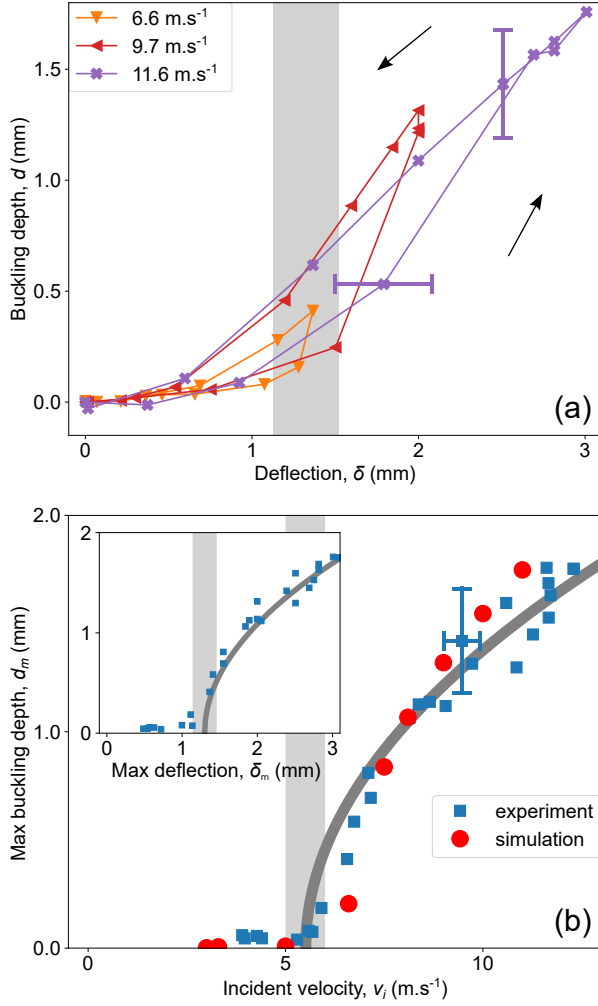


FIG. 5. (a) Depth of the buckle  $d$  vs deflection  $\delta$  and (b) maximum depth  $d_m$  vs incident velocity  $v_i$ . Inset: Maximum depth of the buckle  $d_m$  vs maximum deflection  $\delta_m$ . We observe that the ball shell buckles at a deflection of about  $\delta_c = (1.3 \pm 0.2)$  mm which is reached, in our experiments, for an impact velocity larger than  $v_c = (5.5 \pm 0.5)$  m.s<sup>-1</sup>. Grey vertical lines underline the buckling onset.

plicity, above the onset, the relation is used to get a rough estimate of  $\delta$ . It is of particular interest to display the buckling depth  $d$  as a function of  $\delta$ . In Fig. 5(a), one observes that  $d$  is not a simple function of  $\delta$  but rather exhibits a hysteresis loop. Initially,  $d$  suddenly increases above a threshold,  $\delta_c$ , and then slowly decreases when  $\delta$  decreases back. In spite of this hysteretic behavior, in Fig. 5(b), by reporting the maximum buckling depth  $d_m$  as a function of the incident velocity  $v_i$ , one observes a clear bifurcation that makes it possible to determine precisely the onset,  $v_c$ , of the buckling instability according to the velocity. We obtain  $v_c = (5.5 \pm 0.5)$  m.s<sup>-1</sup>. In Fig. 5(b), inset, one clearly observes that the ball buckles for  $\delta_c \simeq (1.3 \pm 0.2)$  mm, which must be compared to the thickness

of the shell  $h$ . In addition, we estimated using X-ray tomography images that the thickness of the shell is  $(500 \pm 20)$   $\mu$ m. Thus, we find that the critical displacement  $\delta_c$  is indeed of the order of twice the thickness of the shell  $h$  in accordance with the previous results obtained in the quasi-static regime (Appendix A) [6, 9, 11].

In addition, we provide two additional pieces of information by reporting the restitution coefficient  $\varepsilon$  and the contact time  $\tau$  as a function of the incident velocity  $v_i$  (Fig. 6). The restitution coefficient  $\varepsilon$  continuously decreases when the incident velocity,  $v_i$ , is increased but a clear change in regime

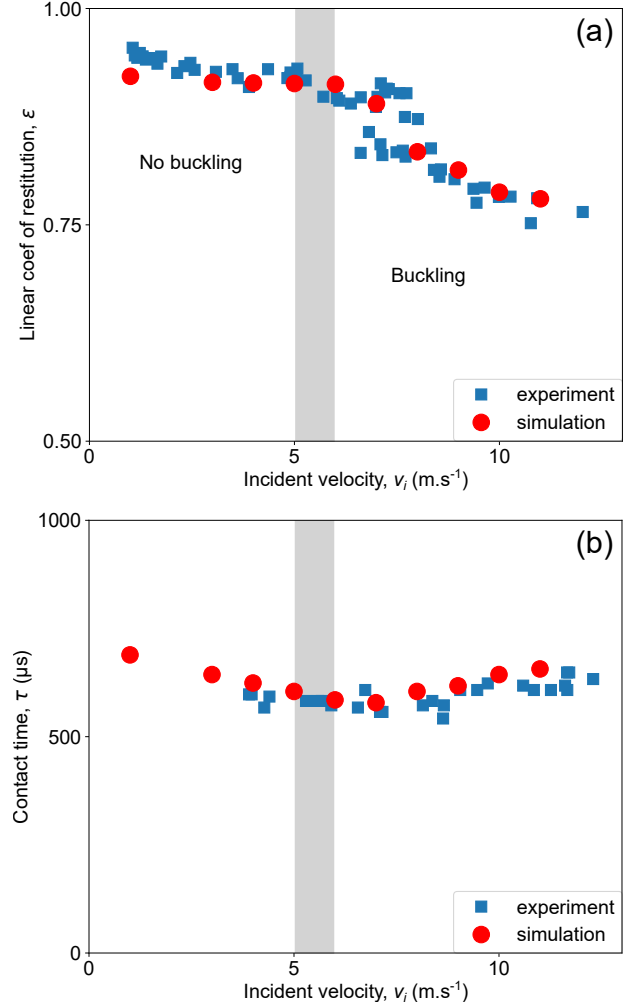


FIG. 6. (a) Restitution coefficient  $\varepsilon$  and (b) contact time  $\tau$  vs incident velocity  $v_i$ . The contact time  $\tau$  shows a slow decrease only at low impact velocities,  $v_i$ , and then when the ball buckles, the contact time increases. By contrast, the restitution coefficient  $\varepsilon$  continuously decreases when the impact velocity,  $v_i$ , is increased and a clear change in regime appears when the ball shell buckles (grey vertical line). We observe a good agreement between numerical and experimental values of both the restitution coefficient  $\varepsilon$  and the contact time  $\tau$  [The error bars are worth the spreading of the experimental points].

is observed in the vicinity of the critical velocity  $v_c$  (Fig. 6a, shaded grey region). The contact time is assessed by considering the number of images in which the diameter  $D \neq 0$ . Over the range of incident velocities explored, one observes that the contact time  $\tau$  decreases slowly until the critical velocity  $v_c$  is reached and then slightly increases (Fig. 6b). For the Hertz contact, the reaction force writes  $F = -k\delta^{3/2}$  where  $k$  accounts for the stiffness of the ball shell. In this framework, the contact time  $\tau \simeq 3.218\left(\frac{m}{k}\right)^{2/5}v_i^{-1/5}$ , where  $m$  is the mass of the ball and  $v_i$  the incident velocity, is expected to decrease slowly when the incident velocity  $v_i$  increases, as observed experimentally as long as the ball shell does not buckle. The subsequent increase of  $\tau$  at large velocity is related to the buckling of the ball shell. This non-monotonic behavior of the contact time  $\tau$  as a function of the incident velocity  $v_i$  has been observed in one previous study [3].

Finally, from the experimental value of the contact time  $\tau \simeq 0.6$  ms, one can estimate the stiffness of the ball (Hertz contact),  $k \simeq 2.5 \cdot 10^6$  N.m $^{-3/2}$  (taking  $m = 2.7$  g and  $v_i = 5.5$  m.s $^{-1}$ ). Neglecting the dissipation, one can then obtain, at the onset of buckling, the maximum deflection  $\delta_c \simeq \left(\frac{5}{4}\frac{m}{k}\right)^{2/5}v_i^{4/5} \simeq 1.1$  mm which nicely compares to the experimental value in regards of the approximation made to obtain this estimate.

In section III, we explain how the numerical simulation of the same system has been carried out and, in section IV, we compare the experimental and numerical results and discuss our findings.

### III. NUMERICAL SIMULATION

#### A. Numerical methods

Explicit 3D Finite Elements (FE) simulations using the commercial software Abaqus<sup>®</sup> are performed to numerically model the normal impact of the ping-pong ball onto the glass substrate [25]. The ball (see Table I for properties) is modeled with 112,903 Shell elements SR4 with five integration points through the thickness. 95,256 C3D8R elements are used for the glass substrate (squared 3D volume). The bottom surface of the glass substrate is fixed. At  $t = 0$  s, the ball and substrate are 0.3 mm apart, and the incident velocity,  $v_i$ , is assigned to the ball (initial condition). Hard normal behavior and an isotropic friction coefficient  $\mu = 0.75$  (penalty) for the tangential behavior define the contact properties. It is worth noting that a quasi-static experiment and a companion FE modelling that are further detailed in Appendix A were used to adjust its value.

Now regarding the material properties, the glass substrate is defined purely elastic (Young modulus  $E_g = 70$  GPa, Poisson ratio  $\nu_g = 0.35$  and density  $\rho_g = 2500$  kg.m $^{-3}$ ). A simple visco-elastic model with a unique discrete Maxwell element was chosen as the simplest model to depict the response of the ball polymeric material (ABS). Indeed, viscous dissipation and a modulus that is time-dependent have to be accounted for [22]. Aside from the density  $\rho_b = 1070$  kg.m $^{-3}$  (back calculated using the ball's dimensions and mass) and the

Poisson ratio  $\nu_b = 0.35$  (typical for polymer materials in the glassy regime) three additional material parameters are then needed: the long time storage modulus  $E_\infty$ , the characteristic time of relaxation  $\tau_1$ , and the elastic modulus  $E_1$  associated to the Maxwell element. Just as the friction coefficient, quasi-static experiments were used to adjust the long time storage modulus and a value of  $E_\infty = (1.5 \pm 0.1)$  GPa was identified (Appendix A). Additionally,  $\tau_1$  was set equal to 0.001 s and  $E_1$  to 0.5 GPa so that the Maxwell element is active for a time coinciding with the dynamical tests and that the amplitude of the relaxation mechanism (i.e. the stiffening) remains consistent with the modulus variation that are often observed in the glassy regime of amorphous thermoplastic polymers.

The simulations are set so that the total energy put into the system equals the initial kinetic energy. With aim to further understand the mechanisms acting during contact, the variations of the contributions to the total energy are monitored: the kinetic energy, the strain energy, the friction dissipation and the viscous dissipation. Typical profiles for these energies are presented in Fig. 7 as a function of time for two chosen incident velocities ( $v_i = 6$  m.s $^{-1}$  and  $v_i = 11$  m.s $^{-1}$ ). At any given time  $t$ , the sum of the energies equals the initial kinetic energy,  $E_{ki}$  (note here that the kinetic and elastic energies are instantaneous values whereas the friction and viscous contributions are losses integrated over time). During contact, the kinetic energy passes through a minimum whereas the strain energy passes through a maximum. Both friction and viscous cumulated contributions are seen to grow with time. At the end of contact, the strain energy almost vanishes for all incident velocities within the accessible range. Thus, the contribution to the dissipation of any subsequent vibrations (clearly revealed at large incident velocity, Fig. 7b), that are later damped by the viscosity, remains small. In any case, this contribution does not play any role in our results as we consider the final translational energy (the average of the kinetic energy over time) after loss of contact which already takes this source of dissipation into account.

Based on these energy profiles, the contact time  $\tau$  and the restitution coefficient  $\varepsilon$  can be determined. On the one hand, the contact time is assessed by tracking the onset and final contact times. At onset, the initial kinetic energy,  $E_{ki}$ , is seen to decrease as it remains constant prior to contact. At the end of contact, the friction dissipation is maximum and remains constant afterwards. On the other hand, the linear coefficient of restitution is obtained by taking the square root of the ratio of the average kinetic energy after contact to the initial kinetic energy of the ball,  $E_{ki}$ .

#### B. Numerical results

We report in Fig. 5b, the maximum buckling depth  $d_m$  from the numerical simulation as function of the incident velocity  $v_i$  and observe a fairly good agreement with the experimental results. In addition, we display in Fig. 6a, the restitution coefficient  $\varepsilon$  as a function of the incident velocity  $v_i$ . The same drop in the values of the coefficient of restitution is observed around the critical velocity  $v_c$ . In Fig. 6b, one observes that

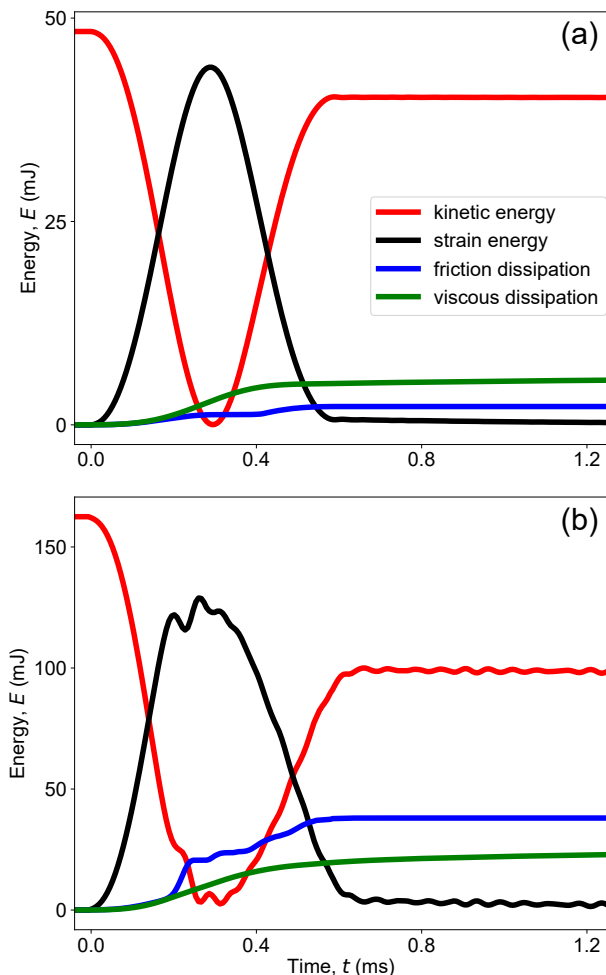


FIG. 7. Different energy contributions vs time  $t$  during a normal impact [(a)  $v_i = 6 \text{ m.s}^{-1}$  and (b)  $v_i = 11 \text{ m.s}^{-1}$ ]. The data are computed from the FE numerical simulation. The kinetic energy decreases to 0 mJ before bouncing back from the surface. There are two sources of energy dissipation: the friction between the shell and the surface in contact, and the energy loss due to the relaxation of the ball material which has a visco-elastic behavior. At any given time, the sum of the energies equals the initial kinetic energy,  $E_{ki}$ , prior to contact. At large velocity (b), one clearly observes the oscillation of the kinetic et strain energies associated with the mechanical vibration of the shell induced by the impact.

the contact time  $\tau$  decreases slowly until the critical velocity  $v_c$  and then slightly increases. In both cases, the agreement with the experimental values is here again good, particularly if one considers that the rheological model used for the ball material is, in this case, simplistic. Indeed, generalized Maxwell model are often employed to capture the distribution of relaxations mechanisms in polymers [26].

Considering the good agreement between experimental and numerical data, we can consider that the numerical simulations account, at least semi-quantitatively, for the experimen-

tal observations. As described in section III A they thus give access to quantities that are not accessible experimentally, in particular, the amounts of energy loaded in the elastic deformation, dissipated by the deformation of the material or by friction. In the section IV, we discuss our experimental findings in the light of the numerical results.

#### IV. DISCUSSION

An elastic spherical shell which collides in normal incidence with a rigid surface deforms and bounces back with a reduced translational velocity, a fraction of the initial kinetic energy,  $E_{ki}$ , being lost during the collision (Fig. 7).

Qualitatively, the deformation of the shell increases with the incident velocity  $v_i$ . Above a critical velocity  $v_c \simeq 5.5 \text{ m.s}^{-1}$ , the surface of the shell elastically buckles in the contact region, the surface of the ball at center leaving the contact with the substrate (Fig. 2). We observe experimentally that the buckling instability occurs when the displacement of the ball towards the solid substrate,  $\delta$ , reaches a critical value which is of about twice the thickness of the ball shell (Fig. 5, here  $\delta_c = (1.3 \pm 0.2) \text{ mm}$  for a shell thickness  $h$  of about  $500 \mu\text{m}$ ). This finding is compatible with the onset of the instability that has been previously determined in quasi-static experiments [11], but yet  $\delta_c$  is larger than twice the thickness of the shell. This result is not surprising as the onset depends on both the Poisson ratio and the friction with the substrate (which tends to delay the onset). More interesting, we measured the same critical value in the quasi-static regime (Appendix A), which clearly demonstrates that the onset of the instability does not significantly change when the impact velocity is increased.

The amount of energy lost during the collision is usually characterized by the restitution coefficient  $\epsilon$ , which corresponds to the ratio between the reflected and the incident linear velocities (Fig. 6). We observe that the restitution coefficient exhibits two regimes as a function of the incident velocity,  $v_i$ , on both sides of the buckling transition. This change in regime has already been observed in previous experiments but we can here associate the transition to the buckling instability [2, 19].

At this point of the discussion, one can ask which of the physical mechanisms contributes to the dissipation. Answering this question is helped by the numerical study (Sec. III). In the numerical simulations, there are three mechanisms that can account for a decrease of the translational velocity:

- The shell is still deformed (even elastically) while leaving the solid surface. In this case, the amount of elastic energy still loaded in the elastic deformation is subtracted from the kinetic energy.
- Due to the visco-elasticity of the shell parent material, the deformation of the ball leads to energy dissipation. This dissipation increases with both the amplitude and rate of the deformation. A part of the incident kinetic energy is dissipated through heat.

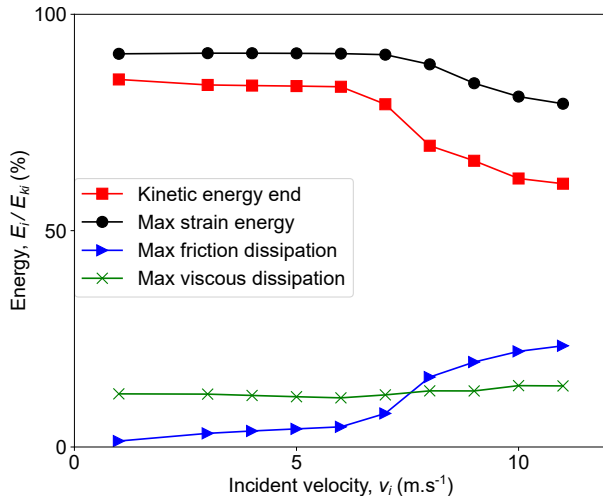


FIG. 8. Relative contributions of the viscous and frictional losses as a function of the incident velocity  $v_i$  - The relative frictional losses increase quickly above the critical velocity  $v_c$  whereas the relative viscous contribution remains constant.

- At the contact between the shell and the solid substrate, energy can be dissipated by friction, meaning that the surfaces in mention are displaced one with respect to the other. This source of dissipation depends on the detailed deformation of the ball and on the normal force in the contact region.

In Fig. 8, we display the contributions listed above, relative to the incident kinetic energy, as a function of the incident velocity  $v_i$ . For clarity, the viscous dissipation includes the first two contributions listed above: the remaining elastic deformation (which anyway will later be dissipated), and the material visco-elasticity.

One can first focus on the dissipation resulting from viscous deformation (Fig. 8). One observes that viscous losses remain almost constant relative to the initial kinetic energy, which means that they increase almost quadratically with the incident velocity. Surprisingly, there is no significant effect of the buckling to this contribution (we remind here that the shell buckles for  $v_i \gtrsim 5.5 \text{ m.s}^{-1}$ ). By contrast, the losses resulting from the friction clearly increase when the shell buckles. The frictional losses are moderate at small velocity  $v_i$ , much smaller than the viscous losses. At larger velocity the frictional losses dominate. The relatively sudden increase of the frictional losses, due to the buckling of the shell, is responsible for the change in regime observed in the behavior of the restitution coefficient  $\epsilon$  as a function of the incident velocity  $v_i$  (Fig. 6a).

## V. CONCLUSION AND PERSPECTIVE

We reported of a series of experiments and a numerical study of the rebound of a spherical shell (a table-tennis ball) impinging in normal incidence on a solid surface (a glass plate). The main conclusions of the studies are that:

- the spherical shell buckles even at relatively small incident velocities, typically  $5.5 \text{ m.s}^{-1}$ , i.e.  $20 \text{ km.h}^{-1}$ .
- the dynamical buckling onset is typically the same as that previously determined in quasi-static experiments. Even at large velocities, the shell buckles when the displacement of the ball towards the solid substrate exceeds about twice the thickness of the shell.
- the restitution coefficient exhibits a change in regime on both sides of the buckling instability. The dissipation is enhanced when the shell buckles and, as a consequence, the restitution coefficient decreases faster with the increase of the incident velocity above the onset.
- at small velocity the main losses are viscous and the friction losses, even though it is not negligible, remain moderate.
- the dissipation by friction increases drastically when the shell buckles whereas viscous losses are not significantly altered by the instability. The enhanced decrease of the restitution coefficient above the onset is thus due to the enhanced frictional losses.

We thus observed the buckling, measured the restitution coefficient and discussed the various sources of dissipation. We limited our study to collisions with a rigid substrate in normal incidence. We are now following two different research lines.

During games, the ball rarely impact the racket normally, and besides, the ball reaches high linear velocities ( $50 \text{ km.h}^{-1}$  or more)[27]. One fundamental question is then that of the buckling instability in oblique incidence. The questions raised are that of the geometry of the contact region, of the onset of the buckling instability, of the restitution coefficient and of the transfer from a pure translation to translation and spin.

One major limitation of our study to someone aiming at providing results that can apply to table-tennis is the use of a solid substrate. We are developing an experimental protocol allowing us to observe the contact region in the case of the collision with a soft substrate.

## ACKNOWLEDGMENTS

TR gratefully acknowledges the GDR Sport & Activit  Physique for its financial support. The authors also thank F. Cabrera and M. Bourgoin for having lent the fast camera to the team.

In memory of L. Manin (1973 - 2021).

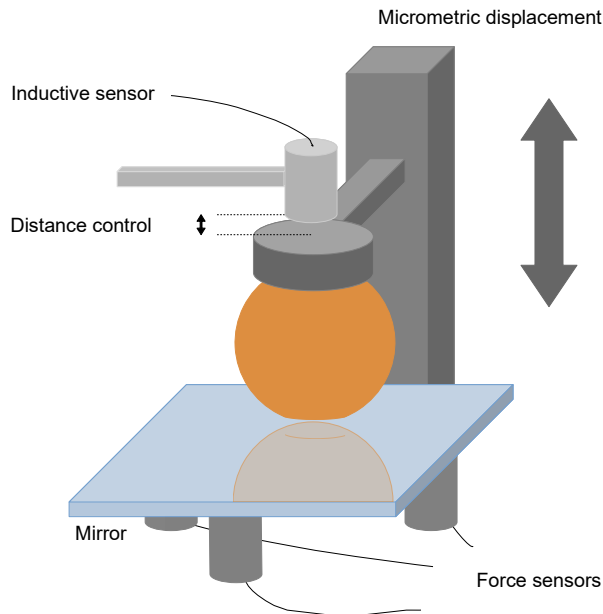


FIG. 9. Sketch of the experimental device – The ball is pushed against a glass window. The displacement is imposed and the resulting force is measured.

#### Appendix A: Quasi-static mechanical response of the ball

We study the mechanical response of the ball by compressing it in a quasi-static manner against a glass window and monitoring both the imposed displacement and the resulting applied force.

The experimental setup (Fig. 9) consists of a horizontal glass mirror lying on three force sensors (Testwell, KD40s  $\pm 200\text{N}$ ) against which the ball is pushed through a horizontal metallic ring. On the one hand, the use of a thick glass mirror (6.5 mm) makes it possible to visually control of the buckling process. On the other hand, the use of the ring avoids any significant localized deformation of the ball at the top. The ring is displaced manually along the vertical axis thanks to a micrometric translation stage (Newport, M-UMR8.25). An inductive sensor (Baumer, IPRM 12I9505/S14), fixed to the ring, provides an accurate measure of the imposed displacement (precision to within  $60\ \mu\text{m}$ ).

The experimental results are reported in Fig. 10 together with the results of the numerical simulations (Sec. III B). We observe two different deforming regimes as a consequence of

the buckling of the ball occurring for  $\delta_c = (1.30 \pm 0.10)\ \text{mm}$ , noticeably and, as expected, of the order of twice the thickness of the shell [6, 11]. The interpolation of the experimental data with the numerical simulations for  $\delta < \delta_c$  gives an estimate of the long time storage modulus,  $E_\infty = (1.5 \pm 0.1)\ \text{GPa}$ , of the shell polymeric material (Fig. 10b). For larger displacements  $\delta$ , when  $\delta > \delta_c$ , the response is seen to be strongly affected by friction and comparison with the numerical results leads

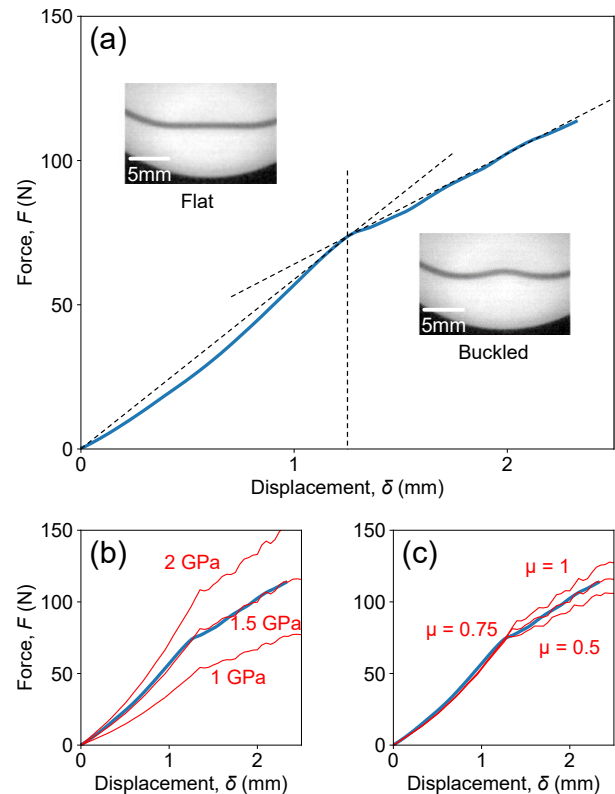


FIG. 10. Force  $F$  vs displacement  $\delta$  – (a) experimental results; interpolations with numerical simulations to estimate (b) the storage modulus and (c) the friction coefficient.

to an estimate of the frictional coefficient  $\mu = (0.75 \pm 0.05)$  (Fig. 10c).

Thanks to these compression tests, we estimated the value of the long time storage modulus,  $E_\infty = 1.5\ \text{GPa}$ , and of the frictional coefficient,  $\mu = 0.75$ , further used in the numerical simulations of the bouncing dynamics.

- 
- [1] J. G. Teng, Buckling of thin shells: Recent advances and trends, *Applied Mechanics Reviews* **49**, 263 (1996).  
 [2] R. H. Bao and T. X. Yu, Collision and rebound of ping pong balls on a rigid target, *Materials & Design* **87**, 278 (2015).  
 [3] M. Hubbard and W. Stronge, Bounce of hollow balls on flat

surfaces, *Sports Engineering* **4**, 49 (2001).

- [4] X. W. Zhang, Z. Tao, and Q. M. Zhang, Dynamic behaviors of visco-elastic thin-walled spherical shells impact onto a rigid plate, *Latin American Journal of Solids and Structures* **11**, 2607 (2014).

- [5] R. G. Rinaldi, L. Manin, S. Moineau, and N. Havard, Table tennis ball impacting racket polymeric coatings: Experiments and modeling of key performance metrics, *Applied Sciences* **9**, 158 (2019).
- [6] R. Kitching, R. Houlston, and W. Johnson, Theoretical and experimental-study of hemispherical shells subjected to axial loads between flat plates, *International Journal of Mechanical Sciences* **17**, 693 (1975).
- [7] J. G. Deoliveira and T. Wierzbicki, Crushing analysis of rotationally symmetric plastic shells, *Journal of Strain Analysis for Engineering Design* **17**, 229 (1982).
- [8] D. P. Updike and A. Kalnins, Axisymmetric behavior of an elastic spherical shell compressed between rigid plates, *Journal of Applied Mechanics* **37**, 635 (1970).
- [9] R. Shorter, J. D. Smith, V. A. Coveney, and J. J. C. Busfield, Axial compression of hollow elastic spheres, *Journal of Mechanics of Materials and Structures* **5**, 693 (2010).
- [10] X.-W. Zhang and T. Yu, Experimental and numerical study on the dynamic buckling of ping-pong balls under impact loading, *International Journal of Nonlinear Sciences and Numerical Simulation* **13**, 81 (2012).
- [11] L. Pauchard and S. Rica, Contact and compression of elastic spherical shells: the physics of a 'ping-pong' ball, *Philosophical Magazine B-Physics of Condensed Matter Statistical Mechanics Electronic Optical and Magnetic Properties* **78**, 225 (1998).
- [12] N. K. Gupta, G. L. E. Prasad, and S. K. Gupta, Axial compression of metallic spherical shells between rigid plates, *Thin-Walled Structures* **34**, 21 (1999).
- [13] D. Karagiozova, X. W. Zhang, and T. X. Yu, Static and dynamic snap-through behaviour of an elastic spherical shell, *Acta Mechanica Sinica* **28**, 695 (2012).
- [14] S. Knoche and J. Kierfeld, Buckling of spherical capsules, *Physical Review E* **84**, 10.1103/PhysRevE.84.046608 (2011).
- [15] N. K. Gupta and Venkatesh, Experimental and numerical studies of dynamic axial compression of thin walled spherical shells, *International Journal of Impact Engineering* **30**, 1225 (2004).
- [16] N. K. Gupta, N. M. Sheriff, and R. Velmurugan, Experimental and numerical investigations into collapse behaviour of thin spherical shells under drop hammer impact, *International Journal of Solids and Structures* **44**, 3136 (2007).
- [17] X. L. Dong, Z. Y. Gao, and T. Yu, Dynamic crushing of thin-walled spheres: An experimental study, *International Journal of Impact Engineering* **35**, 717 (2008).
- [18] N. K. Gupta, N. M. Sheriff, and R. Velmurugan, Experimental and theoretical studies on buckling of thin spherical shells under axial loads, *International Journal of Mechanical Sciences* **50**, 422 (2008).
- [19] R. Cross, Impact behavior of hollow balls, *American Journal of Physics* **82**, 189 (2014).
- [20] I. M. Hutchings, Energy absorbed by elastic-waves during plastic impact, *Journal of Physics D-Applied Physics* **12**, 1819 (1979).
- [21] J. Reed, Energy-losses due to elastic wave-propagation during an elastic impact, *Journal of Physics D-Applied Physics* **18**, 2329 (1985).
- [22] R. G. Rinaldi, L. Manin, C. Bonnard, A. Drillon, H. Lourenco, and N. Havard, Non linearity of the ball/rubber impact in table tennis: experiments and modeling, *Procedia engineering* **147**, 348 (2016).
- [23] W. Schneider, C.A. Rasband and K. Eliceiri, Nih image to imagej: 25 years of image analysis, *Nature Methods* **9**, 671 (2012).
- [24] H. Hertz, Über die berührung fester elastischer körper, *J. für reine und angewandte Mathematik* **92**, 156 (1881).
- [25] M. Smith, *ABAQUS/Standard User's Manual, Version 6.9* (Dassault Systemes Simulia Corp, United States, 2009).
- [26] H. Cho, R. G. Rinaldi, and M. C. Boyce, Constitutive modeling of the rate-dependent resilient and dissipative large deformation behavior of a segmented copolymer polyurea, *Soft Matter* **9**, 6319 (2013).
- [27] S. Rusdorf and G. Brunnett, Real time tracking of high speed movements in the context of a table tennis application, in *Proceedings of the ACM symposium on virtual reality software and technology* (2005) pp. 192–200.
- [28] R. Cross, The bounce of a ball, *American Journal of Physics* **67**, 222 (1999).
- [29] R. Cross, Grip-slip behavior of a bouncing ball, *American Journal of Physics* **70**, 1093 (2002).
- [30] R. Cross, Measurements of the horizontal coefficient of restitution for a superball and a tennis ball, *American Journal of Physics* **70**, 482 (2002).
- [31] C. Y. Wu, L. Y. Li, and C. Thornton, Energy dissipation during normal impact of elastic and elastic-plastic spheres, *International Journal of Impact Engineering* **32**, 593 (2005).
- [32] H. W. Yang, W. B. Guan, and G. Y. Lu, Experimental and numerical investigations into collapse behavior of hemispherical shells under drop hammer impact, *Thin-Walled Structures* **124**, 48 (2018).